CRYSTAL GROWTH & DESIGN

pubs.acs.org/crystal

Article

Open Access

This article is licensed under CC-BY 4.0

New Insights into the Structure and Thermodynamic Stability of Polymorphs I and II of the Nicotinamide:Adipic Acid Co-Crystal: A BEST-CSP Study

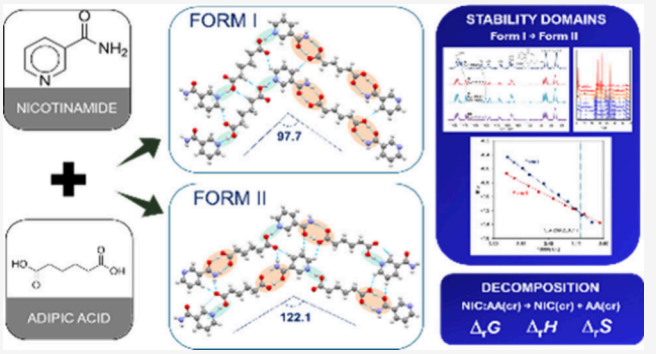
Inês O. Feliciano, Carlos E. S. Bernardes, M. Fátima M. Piedade, M. Soledade C. S. Santos, Paolo P. Mazzeo, Jan Blahut, Martin Dračínský, and Manuel E. Minas da Piedade*

Cite This: *Cryst. Growth Des.* 2026, 26, 5618–5628

Read Online

ACCESS | Metrics & More | Article Recommendations | Supporting Information

ABSTRACT: The polymorphism of the 1:1 nicotinamide:adipic acid (NIC:AA) cocrystal system was re-examined by combining structural and thermodynamic approaches. Differential scanning calorimetry (DSC), solid-state NMR (ssNMR), and variable-temperature powder X-ray diffraction (VT-PXRD) confirmed an enantiotropic relationship between the two polymorphs, evidenced by a direct solid−solid transformation from triclinic form I to monoclinic form II at ∼ 370 K. Solubility data subsequently indicated that this temperature is ∼78 K higher than the equilibrium transition temperature (289.2 ± 0.7 K), consistent with a phase transition hindered by a substantial activation barrier. This also explained why the reverse process was not detected on cooling within the time scale of the DSC, ssNMR, and VT-PXRD experiments. The relative stabilities of forms I and II, as well as their stability relative to dissociation into the coformers, at 298 K, were quantitatively established based on Gibbs energy, enthalpy, and entropy data obtained from solution calorimetry and solubility measurements. The results indicated that at 298 K: (*i*) form II is thermodynamically more stable than form I, despite having a lower lattice enthalpy; (*ii*) this is consistent with the conclusion that the equilibrium transition temperature (289.2 ± 0.7 K) is lower than 298 K and suggests that the stabilization of form II (the high-temperature polymorph) versus form I (low-temperature polymorph) under ambient conditions is of an entropic nature; (*iii*) both polymorphs are stable with respect to dissociation into the coformers nicotinamide and adipic acid; and (*iv*) the stability gain upon cocrystallization is primarily of an enthalpic rather than entropic nature, reflecting a lattice enthalpy advantage relative to the pure components. Single-crystal X-ray diffraction further showed that at ∼298 K form I exhibits an ∼3% higher density and packing index than form II, in line with the observed lattice enthalpy difference $\Delta_{lat}H^{o}_{m}(crI) > \Delta_{lat}H^{o}_{m}(crII)$. Finally, although cocrystallization is frequently used to produce solid forms with enhanced solubility or stability relative to the individual coformers, the formation of the NIC:AA cocrystal does lead to improved solid-state stability but not to solubility enhancement, at least when acetonitrile is used as solvent.

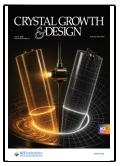


INTRODUCTION

Initially discovered more than a century ago,[1] cocrystallization has been, in recent years, one of the leading strategies to expand the solid form landscape and tune the physicochemical properties of functional organic materials.[2,3] It was once considered that the use of cocrystals could not only provide opportunity for tunning the efficacy of an "active" molecule through selection from a larger number of crystal forms, but also constituted an effective way to avoid polymorphism and the associated complications for manufacturing products with highly reproducible properties.[4] This last conception was rooted on the idea that the noncovalent interactions holding different molecules in a crystal lattice could require more specific packing modes and hinder polymorphic transformations.[5] However, as the number of cocrystals being reported increased, it became apparent that polymorphism was also common in these multicomponent systems.[4,6,7] Similarly to single component crystals, distinct cocrystal polymorphs can display significantly different properties. Thus, strict control over polymorphism is also a *sine qua non* condition for the preparation of cocrystal-based products with highly reproducible properties and function.

Different cocrystal polymorphs can often coexist under the same pressure−temperature conditions, but only one will be

Received: April 24, 2026
Revised: June 5, 2026
Accepted: June 8, 2026
Published: June 23, 2026

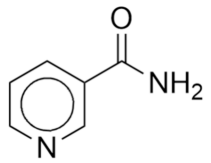


ACS Publications

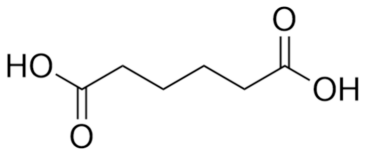
© 2026 The Authors. Published by American Chemical Society

https://doi.org/10.1021/acs.cgd.6c00576
Cryst. Growth Des. 2026, 26, 5618−5628

Downloaded from http://pubs.acs.org/cgdefu/article-pdf/26/14/5618/6521451/acs.cgd.6c00576.pdf by UNIV DEGLI STUDI DI PARMA user on 27 July 2026



Nicotinamide (NIC)



Adipic acid (AA)

Figure 1. Molecular structures of the two coformers used in this work.

thermodynamically stable. In the absence of sufficiently high kinetic barriers metastability cannot be sustained, and all metastable polymorphs will tend to evolve over time to the thermodynamically stable form. Therefore, once cocrystal polymorphism has been identified, structural characterization should be accompanied by a thorough assessment of the relative stability of the different forms in the temperature range of interest for the application in view. An important progress within this scope has been the combination of experimental and *in silico* polymorph screenings. Crystal structure prediction (CSP) methodologies have become of great interest to forecast the stability hierarchy of plausible crystal forms of a given compound. These predictions can considerably help the assessment of manufacture risks associated with polymorphism, thus contributing to avoid the occurrence of serious incidents, as showcased by the ritonavir example.[8] CSP methods have advanced considerably in recent years, and applications have already covered cocrystals.[9−11] Their development requires, however, accurate thermodynamic data (e.g., lattice energies; temperatures, enthalpies, entropies, and Gibbs energies of polymorphic phase transitions or cocrystal dissociation into the precursors) that can be used to benchmark the predictions of structural landscapes and expand potential applications to, for example, the forecast of thermal stability domains or solubilities of different polymorphs.

Experimental Gibbs energy, enthalpy and entropy data for cocrystal dissociation into the precursors are scarce, representative examples being quinidrone,[12] nicotinamide:mandelic acid,[13] felodipine:4,4'-bipyridine,[14] carbamazepine:saccharin,[15] diflunisal:nicotinamide,[16] melatonin:pimelic acid,[17] theophylline:salicylic acid,[18] celecoxib:nicotinamide,[19] fumaric acid:glycine,[20] maleic acid:glycine,[20] maleic acid: L-phenylalanine,[21] and carbamazepine:benzamide.[22] Similar data for polymorphic phase transitions of bi- and multicomponent crystals are even scarcer, and in most cases the performed experiments provide only information on the temperature and enthalpy of the phase transition with a reliability that is impossible to assess. Representative examples include the nicotinamide:(*R*)-mandelic acid,[23] carbamazepine:nicotinamide,[24] and metronidazole benzoate:salicylic acid systems.[25] Addressing this gap is a central goal of COST Action BEST-CSP (Bringing Experiment and Simulation Together in Crystal Structure Prediction), an European initiative combining efforts from experts on CSP and experimentalists working on the determination accurate structural, thermodynamic, and physical property data for a number of model systems, against which the theoretical predictions may be tested.[26]

The present study is part of this effort. It is focused on the nicotinamide (NIC):adipic acid (AA) cocrystal system (Figure 1), which is known to crystallize in two polymorphic forms of 1:1 stoichiometry: the triclinic form I[27] (CSD ref code NUKYIC),[28] and the monoclinic form II[29] (CSD ref code NUKYIC01).[28] Based on calorimetric and solubility measurements the relative stability of both forms, under ambient temperature (298 K) and pressure (1 bar) has been established, on Gibbs energy, enthalpy, and entropy grounds. The experiments also afforded stability relative to decomposition into the precursors. Finally possible structure−stability links were discussed, by combining thermodynamic, X-ray diffraction (single crystal and powder), and solid-state nuclear magnetic resonance information.

MATERIALS AND METHODS

Materials

Solvents. DMSO (Thermo Scientific, HPLC grade, 99.9%), acetonitrile (Honywell, > 99.9%), methanol (Sigma-Aldrich, HPLC grade, > 99.9%), chloroform (Lab-Scan, 99.5%), and ethanol (Carlo Erba, HPLC grade, > 99.9%) were used as received.

Starting Materials. Nicotinamide (NIC, Acros Organics, 99.0%, CAS Nr 98-92-0) was used without further purification. Elemental analysis for $C_6H_6N_2O$ (molar percentage; mean of two determinations): expected C 59.0%, N 22.9%, H 5.0%; found C 58.6 ± 0.3%, N 22.7 ± 0.3%, H 5.1 ± 0.1%. The PXRD pattern obtained at 296 ± 2 K for NIC was indexed as monoclinic, $P2_1/c$, a = 3.972(4) Å, b = 15.636(6) Å, c = 9.418(9) Å, β = 99.06(20)° in good agreement with the single crystal X-ray diffraction data (SCXRD) reported for polymorph I (CSD RefCode: NICOAM05):[28,30] monoclinic, $P2_1/c$, a = 3.97447(1) Å, b = 15.6420(7) Å, c = 9.4298(5) Å, β = 99.0234(29)°. Adipic acid (AA, $C_6H_{10}O_4$, TCI, 99.9%, CAS Nr 124−04−9) was used as received. Elemental analysis for $C_6H_{10}O_4$: expected C 49.3%, H 6.9%; found C 48.8 ± 0.3%, H 6.9 ± 0.1%; PXRD pattern obtained at 296 ± 2 K was indexed as monoclinic, $P2_1/n$, a = 7.364(10) Å, b = 5.178(11) Å, c = 10.029(11) Å, β = 110.66(40)°. This indicated that the sample corresponded to polymorph I (CSD RefCode: ADIPAC14):[28,31] monoclinic, $P2_1/n$, a = 7.3738(17) Å, b = 5.1520(9) Å, c = 10.016(2) Å, β = 110.47(2)°.

Co-Crystal Syntheses. Form I of the nicotinamide:adipic acid (NIC:AA) cocrystal was prepared by mechanochemistry. Equimolar amounts (0.37 mmol; 100 mg of mixture) of nicotinamide and adipic acid were milled for 20 min, at 30 Hz, in a 10 cm^3 stainless-steel jar, with two 10 mm diameter stainless steel balls. The powder pattern of the obtained product, acquired at 296 ± 2 K, was indexed as triclinic, $P\bar{1}$, a = 5.050(2) Å, b = 5.397(2) Å, c = 24.236(10) Å, α = 93.82(3)°, β = 93.66(3)°, γ = 90.99(4)°. These values are in excellent agreement with the single crystal X-ray diffraction (SCXRD) results obtained in this work for form I, at 298 ± 2 K (see below): triclinic, $P\bar{1}$, a = 5.0516(15) Å, b = 5.3999(17) Å, c = 24.260(8) Å, α = 93.996(12)°, β = 93.766(12)°, γ = 90.933(12)°.

The synthesis of the nicotinamide:adipic acid form II polymorph was identical to that described for form I, except that 15 μL of methanol were added to the jar. The powder pattern of the obtained product, acquired at 296 ± 2 K, was indexed as monoclinic, $P2_1/c$, a = 4.978(5), b = 30.268(23) Å, c = 8.935(8) Å, β = 93.68(27)°. These values are in good agreement with the SCXRD results obtained in this work for form II, at 298 ± 2 K (see below), $P2_1/c$, a = 4.981(5) Å, b = 30.35(3) Å, c = 8.932(8) Å, β = 93.76(3)° and previously reported at

Downloaded from http://pubs.acs.org/cgdefu/article-pdf/26/14/5618/6521451/acs.cgd.6c00576.pdf by UNIV DEGLI STUDI DI PARMA user on 27 July 2026

https://doi.org/10.1021/acs.cgd.6c00576
Cryst. Growth Des. 2026, 26, 5618−5628

295 K (CSD RefCode: NUKYIC01),[28,29] monoclinic, $P2_1/c$, a = 4.9815(2) Å, b = 30.3259(19) Å, c = 8.9413(4) Å, β = 93.776(4)°.

Elemental Analysis

Elemental C, H, and N analyses were performed on a Fison Instruments *EA* apparatus, with a typical accuracy error of ± 0.3% for carbon and nitrogen and ±0.1% for hydrogen. These uncertainties are based on interlaboratory tests carried out between national certified laboratories and the ISO 11352/2012 standards.

Powder X-ray Diffraction (PXRD)

Powder X-ray diffraction analyses used in the identification of the crystal forms studied in this work were carried out at 296 ± 2 K, on a Philips X'Pert PRO X-ray diffractometer, operating in the θ-2θ mode. The apparatus was equipped with a PW 3050/60 vertical goniometer and an X'Celerator detector. The radiation was produced with a Cu−Kα (λ = 1.5406 Å) tube, operated at 40 kV and 30 mA. Data were collected in the 5−35° 2θ range, with a step size of 0.017°, and a step duration of 40 s. Aluminum sample holders were used. The indexation of the powder patterns was performed with CelRef.[32]

Variable Temperature Powder X-ray Diffraction (VT-PXRD)

VT-PXRD experiments were performed on both NIC:AA polymorphs, using a Rigaku SmartLab XE diffractometer, equipped with a solid-state Hypix3000 2D detector, and an Anton-Paar TTK600 nonambient chamber. The samples were placed on a flat copper holder and heated in steps, at ambient pressure, holding the sample for thermalization for 1 min before each data acquisition. Data was collected at the following temperatures: 297.9, 313.1, 328.1, 343.1, 358.1, 368.1, 378.1, 383.1, and 388.1 K, for form I; 298.8, 313.1, 328.1, 343.1, 358.1, and 373.1 K, for form II. The powder patterns were collected in 1D mode, in the 5−40° 2θ range, with a scan rate of 10° min^{-1}. A length-limiting slit of 10 mm, compatible with the nonambient chamber, was used to enhance X-ray flux over the sample, while 2.5° soller slits were used to improve the peak profile and limit the overlapping of reflections. Quantitative phase analysis as well as unit cell parameters as a function of temperature were obtained by Rietveld refinement, using TOPAS v6 software.[33]

Single-Crystal X-ray Diffraction (SCXRD)

Crystals of NIC:AA form I suitable for single crystal X-ray diffraction analysis were obtained at ambient conditions (298 ± 2 K; ∼ 1 bar) by solvent evaporation from a saturated solution prepared using the mechanochemical product and a mixture of chloroform (10 mL) and methanol (50 μL). Form II crystals were prepared by heating form I powder above the temperature of the I → II solid−solid phase transition, followed by cooling to room temperature. Bruker D8 Venture and Bruker AXS-KAPPA APEX II diffractometers were used in the study of forms I and II, respectively. Both diffractometers were equipped with monochromated Mo−Kα (λ = 0.71073 Å) radiation sources, operating at 50 kV and 30 mA. The crystals were coated with Paratone-N oil and mounted on a Kapton loop. Data collection was monitored with the Bruker APEX IV software.[34] An empirical absorption correction was enforced using Bruker SADAB[35] and data reduction was done with Bruker SAINT.[36] The structures were solved by intrinsic phasing with Bruker SHELXT-2017[37] and refined by full-matrix-least-squares on F^2 using SHELXL-2017,[38] both programs included in WINGX-Version 2018.3.[39] The atoms were refined with anisotropic thermal parameters. Most of the hydrogen atoms were inserted in calculated positions and allowed to refine riding on the parent carbon atom. A summary of the crystal data, structure solution, and refinement parameters is given in the Supporting Information (Table S7). Structural representations were prepared using Mercury 2025.1.1.[40]

Solid-State Nuclear Magnetic Resonance (ssNMR)

The ssNMR experiments were carried out on a JEOL 600 MHz spectrometer, equipped with a 3.2 mm HX probe, at a 14.1 T field corresponding to a 600 MHz ^{1}H Larmor frequency. The sample was packed in a 3.2 mm zirconia rotor. The ^{13}C{^{1}H} spectra were acquired using a cross-polarization experiment with 5 ms contact time and preacquisition delay set to 1.5 × T_1(^{1}H) (as obtained from ^{1}H saturation recovery experiment). The number of coadded transients ranged from 16 to 256 depending on the sensitivity of the sample at the selected temperature. The chemical shift of the adamantane CH resonance at 37.8 ppm was used as an external secondary reference for calibration of the ^{13}C chemical-shift scale. The ^{1}H and ^{13}C nutation frequencies were 73.3 kHz and 54.1 kHz, respectively. Real sample temperature (including MAS frictional heating) was determined using the chemical shift of ^{207}Pb.[41] All raw data (^{13}C, ^{1}H spectra and ^{1}H saturation recovery experiments) is available in Zenodo.[42]

NMR chemical shift calculations were carried out using the Gauge Including Projector Augmented Wave (GIPAW) method under periodic boundary conditions,[43,44] as implemented in the CASTEP software (version 22.11).[45] CASTEP operates within a density functional theory (DFT) framework, employing pseudopotentials to account for core−electron effects and plane-wave basis sets to represent valence electrons. Before the NMR calculations, the atomic positions within the experimental unit cell were geometry-optimized while keeping the unit-cell parameters fixed. Both the geometry optimization and NMR calculations were performed using the Perdew−Burke−Ernzerhof (PBE) exchange-correlation functional,[46] with a plane-wave energy cutoff of 600 eV. Default ultrasoft, on-the-fly generated pseudopotentials[47] were used throughout. Brillouin zone sampling was conducted using a Monkhorst−Pack k-point grid[48] with a minimum spacing of 0.1 Å^{-1}, and empirical dispersion interactions were accounted for using the Tkatchenko−Scheffler (TS) correction scheme.[49]

Differential Scanning Calorimetry (DSC)

DSC experiments were performed on a PerkinElmer DSC-7. The apparatus was controlled by the PerkinElmer Pyris V. 7.0.0.0110 software, which was also used for data acquisition and analysis. The temperature range and heating rate were 298−435 K and 5 K min^{-1}, respectively. The samples with 1.5−3.5 mg mass were contained in 20 μL aluminum pans (PerkinElmer 0219-0062), hermetically sealed in air. Weighing with a precision of ±0.1 μg was done on a Mettler XP2U ultramicro balance. The purging gas was nitrogen (Praxair 5.0, 99.999%) at a flow rate of 30 cm^3 min^{-1}. The temperature scale of the apparatus was calibrated at the heating rate of the sample measurements using the following standards: benzoic acid (NIST SRM 39j, 99.9996, T_{fus} = 395.50 K), indium (PerkinElmer, 99.999%, T_{fus} = 429.75 K, $\Delta_{fus}h$ = 28.45 J·g^{-1}), lead (GoodFellow, 99.999, T_{fus} = 600.61 K), and zinc (PerkinElmer, 99.999%, T_{fus} = 692.65 K). The calibration of the heat flow scale was based on the standard specific enthalpy of fusion of the indium standard.

Solubility Measurements

Dynamic solubility measurements in acetonitrile were performed with the in-house developed apparatus illustrated in Figure 2. The system was composed of an aluminum block, where a 3 cm^3 glass vial containing the sample and solvent was inserted. The temperature of

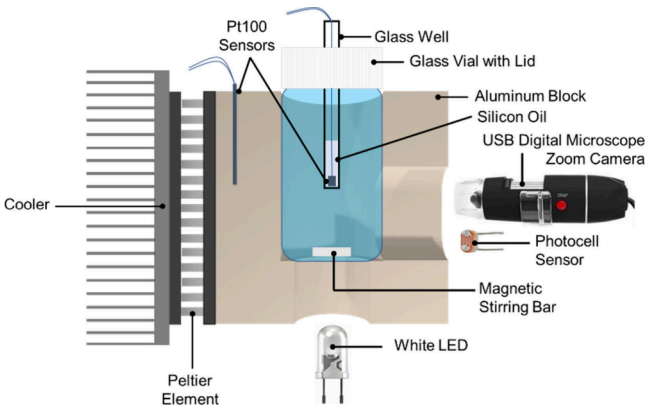


Figure 2. Apparatus used for solubility determinations from dynamic clear point measurements.

https://doi.org/10.1021/acs.cgd.6c00576
Cryst. Growth Des. 2026, 26, 5618−5628

Downloaded from http://pubs.acs.org/cgdefu/article-pdf/26/14/5618/6521451/acs.cgd.6c00576.pdf by UNIV DEGLI STUDI DI PARMA user on 27 July 2026

the block was measured with a RS Pro Pt100 sensor and controlled using a Peltier element (European Thermodynamics GM250-127-14-16), connected to Adafruit MAX31865 and Pololu High-Power Motor Driver 18v15 boards, respectively. The temperature sensor and the motor driver are linked to an Arduino Uno microcontroller, programmed with a PID software specifically designed for this device. This system allows the temperature of the aluminum block to be maintained or increased/decreased at a constant rate, with a precision of ±0.03 K. A white LED illuminates the solution through a hole situated below the sample vessel and the presence or absence of crystals in suspension was simultaneously monitored by two methods: (*i*) a USB Digital Microscope Zoom camera, which captures images of the solution every 1 s and (*ii*) an Advanced Photonix photocell NSL-19M51 sensor (also connected to the Arduino microcontroller) that measures the turbidity of the solution. The temperature of the sample under study was monitored with a second Pt100 probe (TE Connectivity, NB-PTCO-160) inserted in a glass well containing silicon oil, immersed in the solvent. The two Pt100 sensors used in the apparatus were calibrated against a reference Pt100 sensor, which had been previously calibrated at an accredited facility according to the ITS-90 temperature scale. The calibration was performed with the three sensors immersed in water inside the glass vial show in Figure 2. The results indicated that the precision in the measurements of the block and sample temperatures was ± 0.01 K.

In a typical experiment, 5−50 mg of compound and ∼ 1.6 g of acetonitrile (previously placed in a refrigerator at 277 K) were weighed into the glass vial, with a precision of ± 0.01 mg, using a Mettler Toledo XS205 balance. The vial containing the suspension was transferred to the aluminum block, initially kept at 283 K. The sample was subsequently heated at 0.3 K min^{-1}, under magnetic stirring, until complete dissolution of the solid was detected (clear point). The clear point temperature was taken as the average result of the imaging and turbidity measurements. The composition of the mixture was chosen to observe solubilization between 285 and 310 K.

Solution Calorimetry

Enthalpies of solution in DMSO, at 298.15 K, were determined using a previously reported 15.0 cm^3 stainless steel cell adapted to a LKB 2277 Thermal Activity Monitor (TAM).[50] The cell was equipped with a sample holder, sample drop mechanism, stirrer, and electrical calibration system. In a typical experiment, 10−25 mg of sample, gently pressed into a pellet, was weighed with a precision of ± 0.1 μg on a Mettler XP2U ultramicro balance and transferred to the drop chamber of the calorimetric cell. The cell body, containing ∼ 14 g of solvent or solution, was weighed on a Mettler XS205 balance (±10 μg precision) and adjusted to the cell head. The assembled setup was transferred to the calorimeter, and stirring was initiated at 80 rpm. After thermal equilibration and acquisition of the initial baseline, the sample was dropped into the solvent/solution to start the dissolution process. The observed calorimetric curve was monitored until the signal returned to the baseline. The corresponding standard molar enthalpy was calculated from

$$\Delta_{sol}H_m^o = \frac{M}{m}\varepsilon(A - A_b) \quad (1)$$

where A is the area of the measured curve; m and M are the mass and molar mass of the sample, respectively; A_b is the area correction associated with the drop process (i.e., opening the drop chamber without a sample inside), which was determined in independent experiments; and ε is the calibration constant of the calorimeter. The value of ε was obtained from a series of electrical calibrations, where a potential difference, V, was applied to a 20 Ω resistance inside the calorimetric cell, during a predetermined time, t. This caused a current of intensity, I, to flow through the resistance, leading to the dissipation of an amount of heat $Q = VIt$. The calculation of ε was based on $\varepsilon = Q/A_c$, where A_c is the area of the calibration curve. Instrument control and data acquisition were performed using CBCAL 3.0.[51] Data analysis was carried out with EasyGraph II.[52] The accuracy of the electrical calibration had been previously found to be better than 0.06% based on a comparison of the experimentally determined enthalpy of solution of KCl in water ($\Delta_{sol}H_m^o$ = 17.40 ± 0.06 kJ·mol^{-1}; KCl:4115H_2O final solution; mean of 10 independent determinations)[50] and the corresponding value recommended in the NBS Tables ($\Delta_{sol}H_m^o$ = 17.41 ± 0.11 kJ·mol^{-1}).[53]

RESULTS AND DISCUSSION

All molar thermodynamic quantities were calculated based on the molar masses M(NIC:AA) = 268.269 g mol^{-1}, M(NIC) = 122.127 g mol^{-1}, and M(AA) = 146.142 g mol^{-1}, obtained from the 2021 standard atomic masses recommended by the IUPAC Commission.[54] The procedures used in the assignment of uncertainties to the lattice parameters determined by powder and single crystal X-ray diffraction and to all thermodynamic quantities are indicated in the Supporting Information.

Structure

Single-crystal X-ray diffraction structures of NIC:AA have been reported at 180 K for form I (triclinic, CSD RefCode: NUKYIC)[27,28] and at 295 K for form II (monoclinic, CSD RefCode: NUKYIC01).[28,29] The structure of form I was redetermined here, at 298 ± 2 K, to allow direct structural comparison of the two polymorphs at a temperature compatible with the thermodynamic data discussed below, which refer to 298.15 K. For the sake of consistency, the structure of form II was also redetermined at 298 ± 2 K. A summary of the obtained crystal data (full details are given in the Supporting Information) and of the corresponding literature information is given in Table 1.

Table 1. Crystal Data for the Two NIC:AA Polymorphs

	Form I[a]	Form I	Form II[b]	Form II
Refcode or CCDC Nr.	NUKYIC	This work (CCDC 2535150)[c]	NUKYIC01	This work (CCDC 2535152)[c]
T/K	180	298(2)	295	298(2)
Crystal system	Triclinic	Triclinic	Monoclinic	Monoclinic
Space Group	$P\bar{1}$	$P\bar{1}$	$P2_1/c$	$P2_1/c$
a/Å	5.0110(1)	5.0516(15)	4.9815(2)	4.981(5)
b/Å	5.3379(1)	5.3999(17)	30.3259(19)	30.35(3)
c/Å	24.0348(6)	24.260(8)	8.9413(4)	8.932(8)
α/°	93.036(1)	93.996(12)	90	90
β/°	92.753(1)	93.766(12)	93.776(4)	93.76(3)
γ/°	92.189(1)	90.933(12)	90	90
V/Å^3	640.71(2)	658.59(36)	1347.82(12)	1347(2)
Z/Z'	2/1	2/1	4/1	4/1
ρ_{calc}/g cm^{-3}	1.39055(4)	1.3528(7)	1.3221(1)	1.323
k[d]	0.742	0.721	0.688	0.694

[a]References 27, 28. [b]References 28, 29. [c]CCDC number. [d]Values of Kitaigorodskii's packing index, k, were given by Mercury 2025.1.1.[40]

No significant differences were noted between the structural organization of form I at 180 K and 298 ± 2 K (Figure S1, Supporting Information), except for the thermal expansion of the unit cell. The structure of form II here determined at 298 ± 2 K is also in agreement with that previously reported at 295 K (CSD RefCode: NUKYIC01).[28,29] The discussion will, therefore, be focused on the structures of forms I and II at ambient temperature, whose main packing features are illustrated in Figures 3 and 4.

Downloaded from http://pubs.acs.org/cgdefu/article-pdf/26/14/5618/6521451/acs.cgd.6c00576.pdf by UNIV DEGLI STUDI DI PARMA user on 27 July 2026

https://doi.org/10.1021/acs.cgd.6c00576
Cryst. Growth Des. 2026, 26, 5618−5628

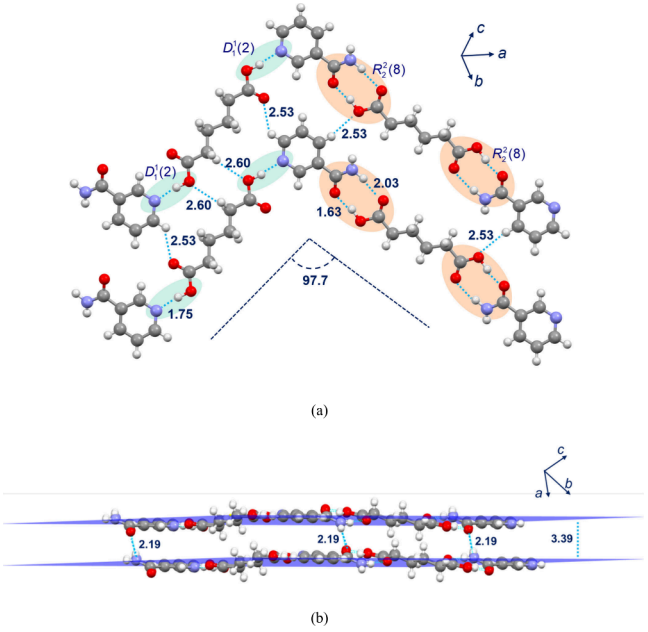


Figure 3. Crystalline structure of NIC:AA form I at 298 ± 2 K (distances in Å): (a) 1D chains sustained by $R_2^2(8)$ and $D_1^1(2)$ motifs and 2D sheets resulting from their interaction through nonclassical C−H···O hydrogen bonds; (b) separation between the layers of 2D sheets forming the 3D packing and intersheet NH···O hydrogen bond.

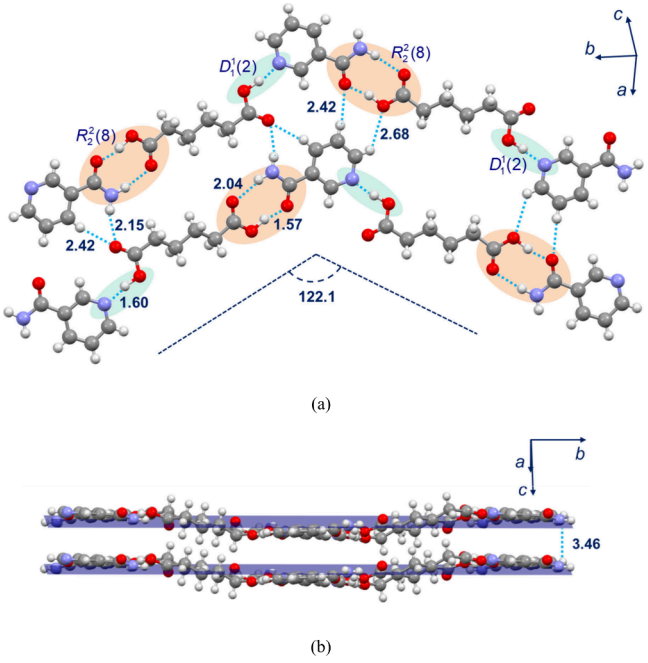


Figure 4. Crystalline structure of NIC:AA form II at 298 ± 2 K (distances in Å): (a) 1D chain sustained by $R_2^2(8)$ and $D_1^1(2)$ motifs and 2D sheets resulting from their interaction through nonclassic C−H···O and N−H···O hydrogen bonds; (b) separation between 2D planes containing the 1D chains in the crystal structure of form II of NIC:AA (distances in Å).

The 1D packing of both polymorphs (Figures 3a and 4a) exhibits infinite *zigzag* chains, where adipic acid and nicotinamide molecules alternate, defining two types of heterosynthons: $D_1^1(2)$ established from an O−H···N hydrogen bond between the AA carboxylic group and the heterocyclic N of NIC; $R_2^2(8)$ involving the COOH group of AA and the $CONH_2$ group of NIC. The chain patterns are, however, different, namely:

Form I: $\mathrm{NIC}^{D_1^1(2)}\,\mathrm{AA}^{D_1^1(2)}\,\mathrm{NIC}^{R_2^2(8)}\,\mathrm{AA}^{R_2^2(8)}\,\mathrm{NIC}$

Form II: $\mathrm{NIC}^{D_1^1(2)}\,\mathrm{AA}^{R_2^2(8)}\,\mathrm{NIC}^{D_1^1(2)}\,\mathrm{AA}^{R_2^2(8)}\,\mathrm{NIC}$

In both forms the 1D chains are linked to each other via an equal number of nonclassical C−H···O hydrogen bonds, forming 2D sheets (Figures 3a and 4a). In form II, however, the sheet framework is further reinforced by a NH···O hydrogen bond ($d_{NH\cdots O}$ = 2.15 Å) between the amidic N−H group of one NIC molecule and the amidic C═O group of a NIC molecule in an adjacent chain (Figure 4a). In form I, the equivalent of the latter type of bond, strengthens the 3D packing which is completed by stacking layers of 2D sheets (Figures 3b and 4b).

On average, the H-bond distances sustaining the $R_2^2(8)$ and $D_1^1(2)$ motifs are slightly longer in form I (Figure 3a: $d_{OH\cdots O}$ = 1.63 Å, $d_{NH\cdots O}$ = 2.03 Å for $R_2^2(8)$ and $d_{OH\cdots N}$ = 1.75 Å for $D_1^1(2)$) than in form II (Figure 4a: $d_{OH\cdots O}$ = 1.57 Å, $d_{NH\cdots O}$ = 2.04 Å for $R_2^2(8)$ and $d_{OH\cdots N}$ = 1.60 Å for $D_1^1(2)$). The C−H···O hydrogen bond interactions sustaining the 2D sheets are also slightly longer, on average, in form I ($d_{CH\cdots O}$ = 2.60 Å, 2.53 Å) than in form II ($d_{CH\cdots O}$ = 2.42 Å, 2.68 Å). These two observations could suggest a higher lattice enthalpy, $\Delta_{lat}H_m^o$, in form II than in form I, in contrast with the calorimetric evidence discussed below, which unequivocally indicated that the opposite is experimentally found. The fact that $\Delta_{lat}H_m^o$ is larger in form I than in form II is, however, consistent with the following results, which indicate a more compact and strong 3D framework in the former than in the latter polymorph: (*i*) the distance between the planes of the 2D sheets is ∼ 2% shorter in form I (3.39 Å, Figure 3b) than in form II (3.46 Å, Figure 4b); (*ii*) the density and the packing index are both ∼ 3% larger in form I than in form II; and (*iii*) the intersheet interactions in form I are most likely strengthened by the presence of the NH···O hydrogen bond mentioned above, which in form II is engaged in 2D interactions.

Thermal Analysis

The thermal behaviors of the two NIC:AA polymorphs and their precursors were investigated through a combination of differential scanning calorimetry (DSC), variable temperature powder X-ray diffraction (VT-PXRD), and solid-state nuclear magnetic resonance (ssNMR) experiments.

Differential Scanning Calorimetry. The DSC results obtained for the NIC:AA polymorphs and their precursors, in the range 298−435 K, at a heating rate of 5 K min^{-1}, are illustrated in Figure 5 and summarized in Table 2 (detailed results are given as Supporting Information). The temperatures of solid−solid phase transition, T_{trs}, or fusion, T_{fus}, in Table 2, refer to the onsets of the observed peaks.

In the case of the monoclinic NIC:AA form II, only a single peak, due to fusion, was detected, at T_{fus} = 397.8 ± 0.2 K, with $\Delta_{fus}H_m^o$ = 52.2 ± 0.3 kJ mol^{-1} and $\Delta_{fus}S_m^o$ = 131.3 ± 0.8 J K^{-1} mol^{-1}. The triclinic form I showed, however, a different DSC pattern. A broad endothermic peak was first detected at T_{trs} = 367.2 ± 0.4 K, with $\Delta_{trs}H_m^o$ = 1.57 ± 0.34 kJ mol^{-1} and $\Delta_{trs}S_m^o$ = 4.29 ± 0.94 J K^{-1} mol^{-1}. Variable-temperature powder X-ray diffraction and solid-state nuclear magnetic resonance analysis (see below) confirmed that this peak corresponded to the form I → form II phase transition, as previously reported.[29] The phase transition peak was followed by a larger and sharper

Downloaded from http://pubs.acs.org/cgdefu/article-pdf/26/14/5618/6521451/acs.cgd.6c00576.pdf by UNIV DEGLI STUDI DI PARMA user on 27 July 2026

https://doi.org/10.1021/acs.cgd.6c00576
Cryst. Growth Des. 2026, 26, 5618−5628

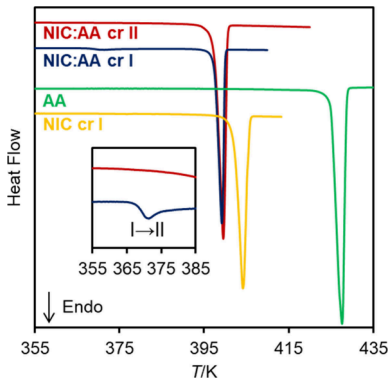


Figure 5. Typical DSC curves obtained for NIC:AA form II (red line), NIC:AA form I (blue line), AA (green line), and NIC form I (yellow line). The inset refers to the temperature range of the NIC:AA form I → form II phase transition.

Table 2. Temperatures, Standard Molar Enthalpies, and Standard Molar Entropies of Fusion and Phase Transition Obtained by DSC for NIC:AA Forms I and II and Their Precursors AA and NIC ($p°$ = 0.1 MPa)[a]

	AA	NIC(crI)[b]	NIC:AA cr I	NIC:AA cr II
T_{fus}/K	424.7 ± 0.5	401.8 ± 0.2	397.6 ± 0.2	397.8 ± 0.2
$\Delta_{fus}H^{o}_{m}$/kJ mol^{-1}	37.1 ± 0.2	23.6 ± 0.1	52.8 ± 0.1	52.2 ± 0.3
$\Delta_{fus}S^{o}_{m}$/J K^{-1} mol^{-1}	87.3 ± 0.6	58.8 ± 0.2	132.8 ± 0.3	131.3 ± 0.8
T_{trs} /K			367.2 ± 0.4[c]	
$\Delta_{trs}H^{o}_{m}$/kJ mol^{-1}			1.57 ± 0.34[c]	
$\Delta_{trs}S^{o}_{m}$/J K^{-1} mol^{-1}			4.29 ± 0.94[c]	

[a]The temperatures of solid−solid phase transitions (T_{trs}) or fusion (T_{fus}) refer to the onsets of the observed peaks. [b]Revised data from reference[57] (see Supporting Information). [c]Form I → Form II phase transition.

endothermic peak due to fusion of form II, as indicated by the close agreement between the obtained T_{fus} = 397.6 ± 0.2 K, $\Delta_{fus}H^{o}_{m}$ = 52.8 ± 0.1 kJ mol^{-1}, and $\Delta_{fus}S^{o}_{m}$ = 132.8 ± 0.3 J K^{-1} mol^{-1}, and the corresponding data mentioned above for the fusion of pure form II. The T_{fus} value obtained for NIC:AA form II (T_{fus} = 397.8 ± 0.2 K) is lower than the temperatures of fusion of both coformers, namely, T_{fus}(AA) = 424.7 ± 0.5 K and T_{fus}(NIC) = 401.9 ± 0.2 K. This observation places the NIC:AA system in the second most abundant group of cocrystals in terms of temperature of fusion (class II; 30−39% relative abundance), for which T_{fus}(cocrystal) < T_{fus}(precursors).[55,56] It can also be noted that the DSC data here obtained for forms I and II agree with the cruder T_{fus} = 400 ± 5 K (n = 2, n is the number of data points considered), T_{trs} = 363 ± 6 K (n = 3), $\Delta_{trs}H^{o}_{m}$ = 1.6 ± 0.2 kJ mol^{-1} (n = 3) calculated by combining published data[29] determined in a single laboratory, at heating rates of 1 K min^{-1} and 5 K min^{-1}, and two different instruments.

Overall, the DSC analysis suggests the two NIC:AA forms are enantiotropically related: polymorph I is thermodynamically stable up to T_{trs}, where stability is reversed and polymorph II becomes the stable form up to fusion. The fact that the form II → form I transformation has been found to take months at ambient temperature and pressure,[29] and it is not observed on cooling in the time scale of a typical DSC experiment, gives a clear indication that the forward and reverse form I ⇌ form II processes are hindered by a significant activation barrier.[58] As a result the transition is only observed on heating (form I → form II), suggesting that the process requires form I to attain considerable metastability. This is consistent with the fact that the onset temperature observed in this work by DSC (T_{trs} = 367.2 ± 0.4 K) is 78 K higher than T_{trs} = 289.2 ± 0.7 K given by the solubility measurements discussed below, which should be representative of equilibrium conditions. This type of behavior is not uncommon,[59] and has been observed, for example, in the case of 4'-hydroxybenzaldehyde and 4'-hydroxyacetophenone.[58,60] Further support for the conclusions of the DSC study was obtained from the results of VT-PXRD and ssNMR experiments.

Variable Temperature Powder X-ray Diffraction (VT-PXRD). VT-PRXD analyses evidenced a progressive transformation of form I to form II between 358 and 383 K (Figure 6), consistent with the crI → crII phase transition temperature

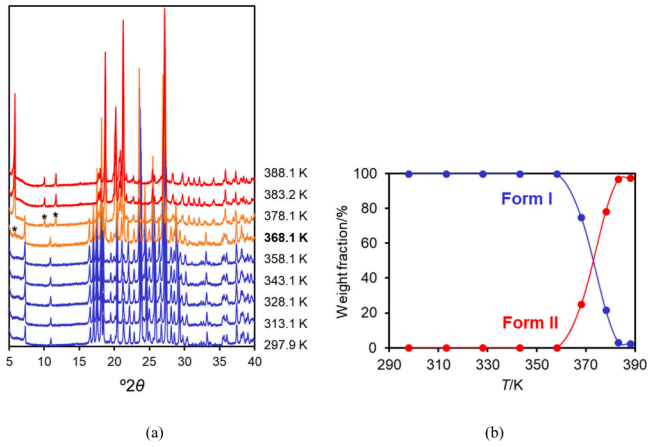


Figure 6. Variable-temperature powder X-ray diffraction results for NIC:AA. (a) Blue patterns refer to form I. Orange patterns refer to conditions where transition from form I to form II has started yet both forms are simultaneously present (* indicates characteristic peaks of form II). Red patterns refer to form II. (b) Quantitative phase analysis performed via Rietveld refinement of the VT-PXRD data, showing the form I → form II phase transition in the range 358−383 K.

found in the DSC experiments (T_{trs} = 367.2 ± 0.4 K). No intermediary phases were detected. Rietveld refinement of the diffraction data, performed with TOPAS,[33] provided the temperature dependence of the specific volume, v, for both polymorphs over the 300−370 K range (see Supporting Information). The v (cm^3 g^{-1}) vs T (K) values were fitted by least-squares regression to the equation:

$$v = v_o(1 + \alpha_V T) \quad (2)$$

where α_V, is the thermal expansion coefficient and v_0 is the specific volume at 0 K. The results and corresponding fitting relationships are illustrated in Figure 7, from which it can be concluded that α_V = (2.57 ± 0.08) × 10^{-4} K^{-1} and v_0 = 0.685 ± 0.002 cm^3 g^{-1} for form I and α_V = (2.81 ± 0.06) × 10^{-4} K^{-1} and v_0 = 0.701 ± 0.002 cm^3 g^{-1} for form II. These values indicate that both polymorphs exhibit positive thermal expansion, and that the corresponding α_V values are ca. 50−60% larger than the average value, α_V = (1.73 ± 0.45) × 10^{-4}

https://doi.org/10.1021/acs.cgd.6c00576
Cryst. Growth Des. 2026, 26, 5618−5628

Downloaded from http://pubs.acs.org/cgdefu/article-pdf/26/14/5618/6521451/acs.cgd.6c00576.pdf by UNIV DEGLI STUDI DI PARMA user on 27 July 2026

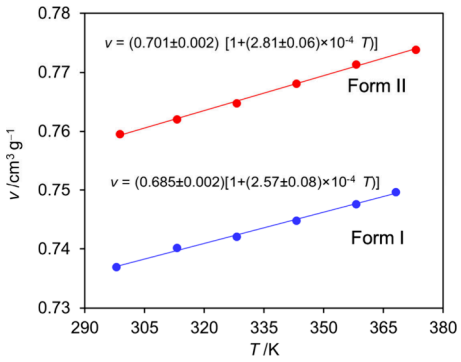


Figure 7. Specific volume of NIC:AA form I (blue) and form II (red) as a function of temperature.

K^{-1},[61] found in a survey of thermal expansion coefficients for organic molecular crystals in the Cambridge Structural Database. Figure 7 also shows that form I has a smaller specific volume than form II at any given temperature. This reflects the larger crystal density and higher lattice enthalpy (see below) of form I compared with form II throughout the temperature range probed, suggesting that the phase transition is solely entropically driven, as generally expected for an enantiotropic polymorphic system.

Solid-State Nuclear Magnetic Resonance (ssNMR). The results of the ssNMR experiments are shown in Figure 8.

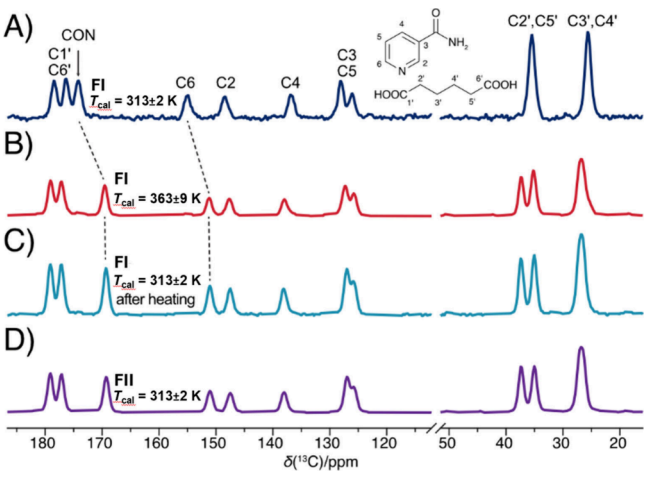


Figure 8. ^{13}C CP-MAS spectra of nicotinamide-adipic acid cocrystals (14.1 T, 18 kHz MAS, contact time 5 ms) for form I measured at temperatures of (a) 313 ± 2 K, (b) 363 ± 9 K, and (c) again at 313 ± 2 K after heating, and (d) for form II at 313 ± 2 K. The signal assignments are based on comparison with DFT-calculated chemical shifts.

The comparison of the spectra of form I acquired near room temperature (313 K, Figure 8a) and at 363 K (Figure 8b) reveals significant spectral changes with temperature, consistent with the occurrence of the form I → form II phase transition. Cooling the sample to 313 K results in minimal spectral variation (Figure 8c), and the spectrum closely matches that of an independently prepared form II sample recorded at the same temperature (Figure 8d).

The most significant chemical-shift differences between the two forms are observed for the carbonyl carbon of NIC, the C6 carbon of NIC, and the CH_2 carbons C2′ and C5′ of AA (see atom labeling in the inset of Figure 8). In form I, the NIC carbonyl group participates in two classical hydrogen bonds: (NIC)C═O−HO(AA), 1.63 Å, in the 2D sheet plane (Figure 3a) and interplanar (NIC)C═O−HN(NIC), 2.19 Å (Figure 3b). In the case of form II, however, only one type of classical hydrogen bond interaction is formed (NIC)C═O−HO(AA), 1.57 Å (Figure 4). This difference is reflected in the deshielding of the carbonyl carbon in form I (i.e., a higher chemical shift, 174 ppm in form I, 169 ppm in form II; DFT calculated values: 172 ppm in form I, 166 ppm in form II). The C6 carbon of NIC is involved in a C−H···O intermolecular hydrogen bond in both forms; however, the shorter contact and larger C−H···O angle in form I result in reduced shielding of this carbon (i.e., 155 ppm in form I, 151 ppm in form II; DFT calculated values: 155 ppm in form I, 149 ppm in form II). Additionally, the two CH_2 carbon atoms adjacent to the COOH groups in AA resonate at the same chemical shift in form I, whereas two distinct signals are observed in form II. A comparison of the most significant hydrogen bond distances and angles computed here by DFT and experimentally found by SCXRD is given in the Supporting Information.

In agreement with the VT-PRXD observations, no intermediate phases were detected during the solid−solid phase transitions. The ssNMR results also corroborate the conclusion from the DSC experiments, that due to a significant activation barrier, the form I → form II process is only observed on heating.

Thermodynamic Stability of the NIC:AA Polymorphs

The relative stability of the two NIC:AA polymorphs and their stabilities relative to decomposition into the NIC(crI) and AA coformers, at 298.15K, were evaluated based on the standard molar Gibbs energy, enthalpy, and entropy changes of the reaction:

$$\text{NIC: AA(cr I/cr II)} \rightarrow \text{NIC(cr)} + \text{AA(cr)} \quad (3)$$

denoted as, $\Delta_r G_m^o(3)$, $\Delta_r H_m^o(3)$, and $T\Delta_r S_m^o(3)$, respectively. The values of $\Delta_r H_m^o(3)$ and $\Delta_r G_m^o(3)$ were obtained from solution calorimetry and solubility measurements, respectively, and the entropic contribution, $T\Delta_r S_m^o(3)$, was calculated from

$$\Delta_r G_m^o = \Delta_r H_m^o - T\Delta_r S_m^o \quad (4)$$

The solubility measurements also provided an estimate of the equilibrium temperature of the form I → form II phase transition.

The standard molar Gibbs energy of reaction 3 was evaluated from the equation:[20]

$$\Delta_r G_m^o(3) = -RT \ln\left(\frac{x_{NIC}x_{AA}}{x'_{NIC}x'_{AA}}\right) \quad (5)$$

where x_{NIC} and x_{AA} are the molar fraction solubilities of NIC and AA in acetonitrile resulting from the dissolution of known amounts of NIC:AA(crI/crII) samples, and x'_{NIC} and x'_{AA} are the corresponding solubilities of the pure coformers. The solubility measurements relied on the apparatus and procedure described in the experimental section. This dynamic technique was selected because once in contact with the solvent, both NIC:AA forms tend to convert to the more stable NIC_2:AA phase.[29] Consequently, equilibrium methods cannot be applied. To ensure that the NIC:AA(crI/crII) samples were stable during the measurements, suspensions of the two polymorphs were stirred in several solvents for ca. 15 min (typical time of an experiment) and then analyzed by PXRD. The results showed that acetonitrile was the best solvent to

Downloaded from http://pubs.acs.org/cgdefu/article-pdf/26/14/5618/6521451/acs.cgd.6c00576.pdf by UNIV DEGLI STUDI DI PARMA user on 27 July 2026

https://doi.org/10.1021/acs.cgd.6c00576
Cryst. Growth Des. 2026, 26, 5618−5628

avoid interference of the transformation into NIC_2:AA (Figure S3 of the Supporting Information). For the sake of consistency x'_{NIC} and x'_{AA} were also determined by the same technique.

Linear least-squares fits of van't Hoff equation:

$$\ln x = \frac{a}{T} + b \tag{6}$$

to the ln x vs $1/T$ data obtained for the two NIC:AA polymorphs led to the results illustrated in Figure 9.

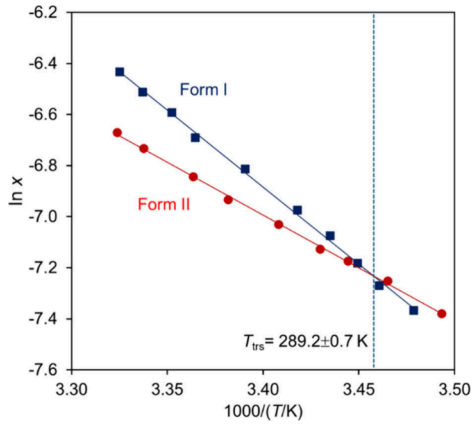


Figure 9. Molar fraction (x) solubilities of NIC:AA forms I (blue) and II (red) in acetonitrile, as a function of temperature (T). The vertical dashed line marks the intersection of the two curves, corresponding to the form I → form II phase transition temperature.

From those linear relationships and analogous counterparts for the coformers (a and b parameters are given in Table S18 of the Supporting Information), the molar fraction solubilities x_{NIC}, x_{AA}, x'^{NIC}, and x'^{AA}, at 298.15 K, in Table 3, were calculated.

Table 3. Results of the Solubility and Calorimetry Measurements on NIC:AA Polymorphs, and Their Co-Formers at 298.15 K

	NIC:AA(crI)	NIC:AA(crII)
$x_{NIC}\times10^3$	1.35 ± 0.05	1.11 ± 0.02
$x_{AA}\times10^3$	1.35 ± 0.05	1.11 ± 0.02
$x'^{NIC}\times10^3$	7.94 ± 0.10	
$x'^{AA}\times10^3$	1.79 ± 0.03	
$\Delta_rG^o_m(3)$/kJ mol^{-1}	5.09 ± 0.28	6.06 ± 0.16
$\Delta_rH^o_m(3)$/kJ mol^{-1}	6.47 ± 0.07	5.09 ± 0.10
$T\Delta_rS^o_m(3)$/kJ mol^{-1}	1.38 ± 0.29	−0.97 ± 0.19
T_{trs}(crI → crII)	289.2 ± 0.7 K	
$\Delta_{trs}G^o_m$(crI → crII)/kJ mol^{-1}	−0.97 ± 0.33	
$\Delta_{trs}H^o_m$(crI → crII)/kJ mol^{-1}	1.38 ± 0.12	
$T\Delta_{trs}S^o_m$(crI → crII)/kJ mol^{-1}	2.35 ± 0.34	
$\Delta_{lat}H^o_m$/kJ mol^{-1}	247.8 ± 0.8	246.4 ± 0.8

To assess the accuracy of the dynamic solubility measurements the solubilities of pure NIC and AA were also determined under equilibrium conditions, at 296.05 ± 0.02 K, using the gravimetric method (see Supporting Information for details). The mean values obtained $\overline{x}_{NIC} = (7.89 \pm 0.22) \times 10^{-3}$ and $\overline{x}_{AA} = (1.76 \pm 0.01) \times 10^{-3}$ differ by 8.4% and 9.7%, respectively, from $x_{NIC} = (7.23 \pm 0.09) \times 10^{-3}$ and $x_{AA} = (1.59 \pm 0.03) \times 10^{-3}$ calculated at the same temperature, using eq 6 and the values of the a and b parameters for NIC and AA in Table S18 of the Supporting Information. Substitution of the x_{NIC}, x_{AA}, x'_{NIC}, and x'_{AA} values in Table 3 into eq 5 led to the $\Delta_rG^o_m(3)$ values that are also given in Table 3, from which the Gibbs energy of the form I → form II phase transition at 298.15 K, could be derived as $\Delta_{trs}G^o_m$(crI → crII) = $\Delta_rG^o_m$(3, crI) − $\Delta_rG^o_m$(3, crII) = −0.97 ± 0.33 kJ mol^{-1} (Table 3). Two main conclusions can be drawn from these results: (*i*) the fact that, at 298.15 K, $\Delta_rG^o_m(3)$ is always positive implies that, around ambient temperature and pressure, both NIC:AA polymorphs are stable relative to decomposition into the precursors; (*ii*) the negative value of $\Delta_{trs}G^o_m$(crI → crII) indicates that the form I to form II transition is thermodynamically favored at that temperature. This is consistent with the prediction from the intersection of the solubility curves in Figure 9, that the crI → crII transition should occur at a temperature close to ambient conditions, namely T_{trs} = 289.2 ± 0.7 K (Table 3 and Figure 9). It is also worth recalling (see discussion of the DSC results) that the latter value, which corresponds to an estimate of the equilibrium temperature of the transition, is 78 K lower than the result obtained by DSC (T_{trs} = 367.2 ± 0.4 K, Table 2).

The standard molar enthalpy of reaction 3, $\Delta_rH^o_m(3)$, was obtained from isothermal calorimetry measurements of the enthalpies of the dissolution processes:

$$\text{NIC: AA(crI/II)} + \text{2011DMSO(l)} \rightarrow \text{[NIC + AA + 2011DMSO](sln)} \tag{7}$$

$$\text{AA(cr)} + \text{2011DMSO(l)} \rightarrow \text{[AA + 2011DMSO](sln)} \tag{8}$$

$$\text{NIC(cr)} + \text{[AA + 2011DMSO](sln)} \rightarrow \text{[NIC + AA + 2011DMSO](sln)} \tag{9}$$

The corresponding results (see Supporting Information for details), $\Delta_{sol}H^o_m$(7, crI) = 26.58 ± 0.04 kJ mol^{-1}, $\Delta_{sol}H^o_m$(7, crII) = 25.20 ± 0.08 kJ mol^{-1}, $\Delta_{sol}H^o_m$(8) = 9.41 ± 0.05 kJ mol^{-1}, and $\Delta_{sol}H^o_m$(9) = 10.70 ± 0.03 kJ mol^{-1} led to the $\Delta_{sol}H^o_m(3)$ values in Table 3, based on the equation:

$$\Delta_rH^\circ_m(3, \text{crI/crII}) = \Delta_{sol}H^\circ_m(7, \text{crI/crII}) - \Delta_{sol}H^\circ_m(8) - \Delta_{sol}H^\circ_m(9) \tag{10}$$

From the $\Delta_rH^o_m(3)$ results it is also possible to obtain the enthalpy of the form I → form II phase transition as: $\Delta_{trs}H^o_m$(crI → crII) = $\Delta_rH^o_m$(3, crI) − $\Delta_rH^o_m$(3, crII) = 1.38 ± 0.12 kJ mol^{-1}. Finally, the entropy terms, $T\Delta_rS^o_m(3)$ and $T\Delta_{trs}S^o_m$(crI → crII) could be derived from eq 4 by using the corresponding Gibbs energy and enthalpy data in Table 3. The fact that for both NIC:AA polymorphs $\Delta_rH^o_m(3) > |T\Delta_rS^o_m(3)|$, indicates that, as most commonly found,[11] the larger stability of these cocrystals relative to the coformers is essentially of enthalpic origin, reflecting a lattice enthalpy gain when the cocrystals form as illustrated in Figure 10. The lattice enthalpies of NIC:AA(crI/crII) are addressed in the following section.

Lattice Enthalpies of the NIC:AA Polymorphs

The lattice enthalpies, $\Delta_{lat}H^o_m$, of NIC:AA(crI/crII), at 298.15 K, were calculated from

Downloaded from http://pubs.acs.org/cgdefu/article-pdf/26/14/5618/6521451/acs.cgd.6c00576.pdf by UNIV DEGLI STUDI DI PARMA user on 27 July 2026

https://doi.org/10.1021/acs.cgd.6c00576
Cryst. Growth Des. 2026, 26, 5618−5628

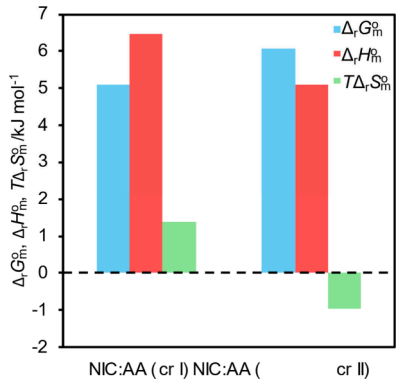


Figure 10. Comparison of the Gibbs energies, enthalpies, and entropies of reaction 3 (see also Table 3) for forms I and II of NIC:AA at 298.15 K.

$$\Delta_{lat}H^o_m(\text{crI/crII}) = \Delta_r H^o_m(3, \text{crI/crII}) + \Delta_{sub}H^o_m(\text{NIC}) + \Delta_{sub}H^o_m(\text{AA}) \quad (11)$$

which can be deduced from the thermodynamic cycle in Figure 11. By using the $\Delta_r H^o_m(3, \text{crI/crII})$ values in Table 3, together

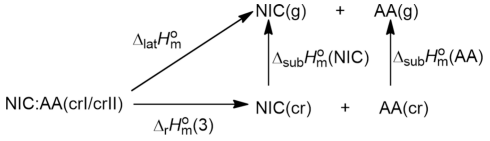


Figure 11. Thermodynamic cycle used to obtain the lattice enthalpies of the NIC:AA polymorphs.

with the previously reported enthalpy of sublimation of nicotinamide, $\Delta_{sub}H^o_m(\text{NIC}) = 108.0 \pm 0.5$ kJ mol^{-1},[57] and the enthalpy of sublimation of adipic acid, $\Delta_{sub}H^o_m(\text{AA}) = 133.3 \pm 0.6$ mol^{-1}, determined in this work (see Supporting Information) it was possible to obtain the lattice enthalpies of the two NIC:AA polymorphs summarized in Table 3. These values exceed the sum of the lattice enthalpies of pure NIC and AA (taken as their enthalpies of sublimation), by 6.5 kJ mol^{-1} for NIC:AA(crI) and 5.1 kJ mol^{-1} for NIC:AA(crII), reflecting the enthalpy gains associated with the formation of the cocrystals expressed by $\Delta_r H^o_m(3, \text{crI/crII})$.

CONCLUSION

The polymorphism of the 1:1 nicotinamide−adipic acid cocrystal system (NIC:AA) was re-examined from structural and thermodynamic perspectives. Calorimetric and solubility measurements confirmed an enantiotropic relationship between forms I and II and enabled a quantitative assessment of their thermal stability domains, as well as their stabilities with respect to dissociation into the individual coformers. Overall, the thermodynamic analysis indicates that at 298 K: (*i*) both NIC:AA polymorphs are stable relative to dissociation into nicotinamide and adipic acid; (*ii*) stability is predominantly enthalpy-driven rather than entropy-driven, consistent with a net gain in lattice enthalpy upon cocrystal formation; and (*iii*) the form I → form II transformation is thermodynamically favored. The solubility studies further suggested that (*iv*) the equilibrium transition temperature is substantially lower (by ∼ 78 K) than the transition temperature inferred from DSC, solid-state NMR, or variable-temperature PXRD.

Single-crystal X-ray diffraction showed that at ∼ 298 K (*v*) form I has both a higher density (∼3%) and a higher packing index (∼3%) than form II, consistent with the relative lattice-enthalpy ordering, $\Delta_{lat}H^o_m(\text{crI}) > \Delta_{lat}H^o_m(\text{crII})$, observed at this temperature. Variable-temperature PXRD additionally revealed that both polymorphs exhibit thermal expansion coefficients that are approximately 50−60% higher than the average value reported from an analysis of Cambridge Structural Database data.

Finally, although cocrystallization is frequently pursued as a strategy to improve solubility and other physicochemical properties of organic functional materials, in the present case, the formation of NIC:AA does lead to a crystal form thermodynamically more stable than the individual coformers, but without any solubility benefit, at least when the solvent is acetonitrile. Indeed, depending on the NIC:AA polymorph the molar fraction solubilities of NIC and AA in this solvent were found to be lower by 83−86% and 26−38%, respectively, than for pure NIC and AA.

ASSOCIATED CONTENT

Supporting Information

The Supporting Information is available free of charge at https://pubs.acs.org/doi/10.1021/acs.cgd.6c00576.

Tables S1−S4 with the indexation of the powder patterns corresponding to various samples mentioned in the text. Tables S5 and S6 with the VT-XRPD data. Table S7 and Figure S1 with SCXRD results. Figure S2 with a comparison of experimental and calculated ^{13}C NMR spectra of forms I and II of nicotinamide-adipic acid cocrystals and magres files from the GIPAW calculations. Table S8 with a comparison of DFT computed hydrogen bond distances and angles and corresponding SCXRD results. Tables S9−S12 with detailed results of the DSC experiments. Tables S13−S16 with detailed results of the solution calorimetry experiments. Tables S17−S19 and Figure S3 with results related to the solubility experiments. Tables S20−S23 with the results of the enthalpy of sublimation measurements on adipic acid by Calvet microcalorimetry. Details of the assignment of uncertainties (Figure S4 and Tables S24 and S25). CIF files with single crystal X-ray diffraction structures of the two NIC:AA polymorphs at 298(2) K, deposited at the Cambridge Crystallographic Data Center (CCDC) with reference numbers 2535150 (form I) and 2535152 (form II) (PDF)

Accession Codes

Deposition Numbers 2535150 and 2535152 contain the supplementary crystallographic data for this paper. These data can be obtained free of charge via the joint Cambridge Crystallographic Data Centre (CCDC) and Fachinformationszentrum Karlsruhe Access Structures service.

AUTHOR INFORMATION

Corresponding Author

Manuel E. Minas da Piedade − *Centro de Química Estrutural, Institute of Molecular Sciences, Departamento de Química e Bioquímica, Faculdade de Ciências, Universidade de Lisboa, 1749-016 Lisboa, Portugal;* orcid.org/0000-0001-7550-6952; Email: memp@fc.ul.pt

Downloaded from http://pubs.acs.org/cgdefu/article-pdf/26/14/5618/6521451/acs.cgd.6c00576.pdf by UNIV DEGLI STUDI DI PARMA user on 27 July 2026

https://doi.org/10.1021/acs.cgd.6c00576
Cryst. Growth Des. 2026, 26, 5618−5628

Authors

Inês O. Feliciano − *Centro de Química Estrutural, Institute of Molecular Sciences, Departamento de Química e Bioquímica, Faculdade de Ciências, Universidade de Lisboa, 1749-016 Lisboa, Portugal*

Carlos E. S. Bernardes − *Centro de Química Estrutural, Institute of Molecular Sciences, Departamento de Química e Bioquímica, Faculdade de Ciências, Universidade de Lisboa, 1749-016 Lisboa, Portugal;* orcid.org/0000-0003-1490-9728

M. Fátima M. Piedade − *Centro de Química Estrutural, Institute of Molecular Sciences, Departamento de Química e Bioquímica, Faculdade de Ciências, Universidade de Lisboa, 1749-016 Lisboa, Portugal*

M. Soledade C. S. Santos − *Centro de Química Estrutural, Institute of Molecular Sciences, Departamento de Química e Bioquímica, Faculdade de Ciências, Universidade de Lisboa, 1749-016 Lisboa, Portugal;* orcid.org/0000-0002-3269-1278

Paolo P. Mazzeo − *Department of Chemical Science, Live Science and Environmental Sustainability, University of Parma, 43124 Parma, Italy;* orcid.org/0000-0002-5787-3609

Jan Blahut − *Institute of Organic Chemistry and Biochemistry, Czech Academy of Science, 160 00 Prague, Czech Republic*

Martin Dračínský − *Institute of Organic Chemistry and Biochemistry, Czech Academy of Science, 160 00 Prague, Czech Republic;* orcid.org/0000-0002-4495-0070

Complete contact information is available at: https://pubs.acs.org/10.1021/acs.cgd.6c00576

Notes

The authors declare no competing financial interest.

■ ACKNOWLEDGMENTS

Centro de Química Estrutural is a Research Unit funded by Fundação para a Ciência e a Tecnologia (FCT) through projects UID/00100/2025 (10.54499/UID/00100/2025), UID/PRR/00100/2025 (10.54499/UID/PRR/00100/2025), and UID/PRR2/00100/2025; (DOI 10.54499/UID/PRR2/00100/2025). Institute of Molecular Sciences is an Associate Laboratory funded by FCT through project LA/P/0056/2020 (10.54499/LA/P/0056/2020). Further support from FCT through project 2023.12474.PEX (10.54499/2023.12474.PEX), a PhD grant awarded to Inês Feliciano (10.54499/2021.04637.BD), and funding to Carlos Bernardes with cofunding from PRR, República Portuguesa and Next Generation EU (contract 2023.15441.TENURE.004/CP00003/CT00002) is also gratefully acknowledged. The ssNMR work was supported by the Ministry of Education, Youth and Sports of the Czech Republic, through the Inter-COST program (ID: LUC24101). The VT-XRPD experiments were supported by COST Action CA22107 (BEST-CSP) and also benefitted from the equipment and framework of the COMP-HUB and COMP-R Initiatives, funded by the 'Departments of Excellence' program of the Italian Ministry for University and Research (MIUR, 2018−2022 and MUR, 2023−2027). Thanks, are finally due to Dr. Franziska Emmerling (BAM, Berlin) for the collection of single crystal X-ray diffraction data on NIC:AA form I at her laboratory.

■ REFERENCES

(1) Wöhler, F. Untersuchungen uber das Chinon. *Analen Chem. Pharm.* **1844**, *51*, 145−163.

(2) Desiraju, G. R.; Vittal, J. J.; Ramanan, A. *Crystal Engineering: A Textbook*; World Scientific Publishing, 2011.

(3) Bacchi, A.; Mazzeo, P. P. Cocrystallization as a Tool to Stabilize Liquid Active Ingredients. *Crystallogr. Rev.* **2021**, *27*, 102−123.

(4) Aitipamula, S.; Chow, P. S.; Tan, R. B. H. Polymorphism in Cocrystals: A Review and Assessment of its Significance. *CrystEngComm* **2014**, *16*, 3451−3465.

(5) Acebedo-Martínez, F. J.; Alarcón-Payer, C.; Frontera, A.; Barbas, R.; Prohens, R.; Di Crisci, M.; Dominguez-Martín, A.; Gómez-Morales, J.; Choquesillo-Lazarte, D. Novel Polymorphic Cocrystals of the Non-Steroidal Anti-Inflammatory Drug Niflumic Acid: Expanding the Pharmaceutical Landscape. *Pharmaceutics* **2021**, *13*, 2140.

(6) Bolla, G.; Sarma, B.; Nangia, A. K. Crystal Engineering of Pharmaceutical Cocrystals in the Discovery and Development of Improved Drugs. *Chem. Rev.* **2022**, *122*, 11514−11603.

(7) Liang, X. X.; Larsen, A. S.; Hans, P.; Xu, D.; Li, Y. X.; Martins, I. C. B.; Rades, T.; Jiang, Y. B. Recent Developments on Co-crystal Polymorphs: From Formation to Prediction. *CrystEngComm* **2025**, *27*, 6415−6432.

(8) Iuzzolino, L.; Kelly, A. W.; Chaudhry, M. T.; Jandl, C.; Stam, D.; Lee, A. Y. Predicting the Ritonavir Crisis by Revisiting the Polymorph Landscape with Crystal Structure Prediction and Form 4 Structure Solution. *Commun. Chem.* **2025**, *8*, 404.

(9) Hunnisett, L. M.; Francia, N.; Nyman, J.; Abraham, N. S.; Aitipamula, S.; Alkhidir, T.; Almehairbi, M.; Anelli, A.; Anstine, D. M.; Anthony, J. E.; et al. The Seventh Blind Test of Crystal Structure Prediction: Structure Ranking Methods. *Acta Crystallogr. B* **2024**, *80*, 548−574.

(10) Hunnisett, L. M.; Nyman, J.; Francia, N.; Abraham, N. S.; Adjiman, C. S.; Aitipamula, S.; Alkhidir, T.; Almehairbi, M.; Anelli, A.; Anstine, D. M.; et al. The Seventh Blind test of Crystal Structure Prediction: Structure Generation Methods. *Acta Crystallogr. B* **2024**, *80*, 517−547.

(11) Taylor, C. R.; Day, G. M. Evaluating the Energetic Driving Force for Cocrystal Formation. *Cryst. Growth Des.* **2018**, *18*, 892−904.

(12) Suzuki, K.; Seki, S. Physicochemical Studies of Molecular Compounds. IV. Heats of Solution of Crystalline Quinone, Hydroquinone and Quinidrone into Acetone and Heat of Formation of Crystalline Quinhydrone. *Bull. Chem. Soc. Jpn.* **1953**, *26*, 372−380.

(13) Zhang, S. W.; Guzei, I. A.; de Villiers, M. M.; Yu, L.; Krzyzaniak, J. F. Formation Enthalpies and Polymorphs of Nicotinamide-*R*-Mandelic Acid Co-Crystals. *Cryst. Growth Des.* **2012**, *12*, 4090−4097.

(14) Surov, A. O.; Solanko, K. A.; Bond, A. D.; Bauer-Brandl, A.; Perlovich, G. L. Polymorphism of Felodipine Co-crystals with 4,4 '-Bipyridine. *CrystEngComm* **2014**, *16*, 6603−6611.

(15) Oliveira, M. A.; Peterson, M. L.; Davey, R. J. Relative Enthalpy of Formation for Co-Crystals of Small Organic Molecules. *Cryst. Growth Des.* **2011**, *11*, 449−457.

(16) Évora, A. O. L.; Castro, R. A. E.; Maria, T. M. R.; Silva, M. R.; ter Horst, J. H.; Canotilho, J.; Eusébio, M. E. S. A Thermodynamic Based Approach on the Investigation of a Diflunisal Pharmaceutical Co-crystal with Improved Intrinsic Dissolution Rate. *Int. J. Pharmaceut.* **2014**, *466*, 68−75.

(17) Yan, Y.; Chen, J. M.; Lu, T. B. Thermodynamics and Preliminary Pharmaceutical Characterization of a Melatonin-Pimelic acid Cocrystal Prepared by a Melt Crystallization Method. *CrystEngComm* **2015**, *17*, 612−620.

(18) Zhang, S.; Chen, H.; Rasmuson, A. C. Thermodynamics and Crystallization of a Theophylline-Salicylic Acid Cocrystal. *CrystEngComm* **2015**, *17*, 4125−4135.

(19) Zhang, S. W.; Brunskill, A. P. J.; Schwartz, E.; Sun, S. Celecoxib-Nicotinamide Cocrystal Revisited: Can Entropy Control Cocrystal Formation? *Cryst. Growth Des.* **2017**, *17*, 2836−2843.

Downloaded from http://pubs.acs.org/cgdefu/article-pdf/26/14/5618/6521451/acs.cgd.6c00576.pdf by UNIV DEGLI STUDI DI PARMA user on 27 July 2026

(20) Évora, A. O. L.; Bernardes, C. E. S.; Piedade, M. F. M.; Conceição, A. C. L.; Minas da Piedade, M. E. Energetics of Glycine Cocrystal or Salt Formation with Two Regioisomers: Fumaric Acid and Maleic Acid. *Cryst. Growth Des.* **2019**, *19*, 5054−5064.
(21) Feliciano, I. O.; Silva, D. P.; Piedade, M. F. M.; Bernardes, C. E. S.; Minas da Piedade, M. E. First and Second Dissociation Enthalpies in Bi-Component Crystals Consisting of Maleic Acid and *L*-Phenylalanine. *Molecules* **2021**, *26*, 5714−5731.
(22) Manin, A. N.; Boycov, D. E.; Simonova, O. R.; Volkova, T. V.; Churakov, A. V.; Perlovich, G. L. Formation Thermodynamics of Carbamazepine with Benzamide, Para-Hydroxybenzamide and Isonicotinamide Cocrystals: Experimental and Theoretical Study. *Pharmaceutics* **2022**, *14*, 1881.
(23) Zhang, S. W.; Harasimowicz, M. T.; de Villiers, M. M.; Yu, L. Cocrystals of Nicotinamide and (*R*)-Mandelic Acid in Many Ratios with Anomalous Formation Properties. *J. Am. Chem. Soc.* **2013**, *135*, 18981−18989.
(24) Buanz, A. B. M.; Parkinson, G. N.; Gaisford, S. Characterization of Carbamazepine-Nicotinamide Cocrystal Polymorphs with Rapid Heating DSC and XRPD. *Cryst. Growth Des.* **2011**, *11*, 1177−1181.
(25) Saraiva Costa, W.; Santiago de Oliveira, Y.; Ayala, A. P. Polymorphism in Cocrystals of Metronidazole Benzoate. *CrystEngComm* **2023**, *25*, 4716−4728.
(26) Wood, W. P.; Arhangelskis, M.; Bartůňková, E.; Bernardes, C. E. S.; Boese, A. D.; Braun, D. E.; Bučar, D. K.; Butkiewicz, H.; Červinka, C.; Civalleri, B.; et al. BEST-CSP Benchmark Study of Polymorphs I and II of Sulfamerazine and the Perils of Polytype Polymorphs. *Cryst. Growth Des.* **2026**, *26*, 476−493.
(27) Karki, S.; Friscic, T.; Jones, W. Control and Interconversion of Cocrystal Stoichiometry in Grinding: Stepwise Mechanism for the Formation of a Hydrogen-Bonded Cocrystal. *CrystEngComm* **2009**, *11*, 470−481.
(28) Groom, C. R.; Bruno, I. J.; Lightfoot, M. P.; Ward, S. C. The Cambridge Structural Database. *Acta Crystallogr. B* **2016**, *72*, 171−179.
(29) Germann, L. S.; Arhangelskis, M.; Etter, M.; Dinnebier, R. E.; Friščić, T. Challenging the Ostwald Rule of Stages in Mechanochemical Cocrystallisation. *Chem. Sci.* **2020**, *11*, 10092−10100.
(30) Fábián, L.; Hamill, N.; Eccles, K. S.; Moynihan, H. A.; Maguire, A. R.; McCausland, L.; Lawrence, S. E. Cocrystals of Fenamic Acids with Nicotinamide. *Cryst. Growth Des.* **2011**, *11*, 3522−3528.
(31) Bhattacharya, S.; Saraswatula, V. G.; Saha, B. K. Thermal Expansion in Alkane Diacids - Another Property Showing Alternation in an Odd-Even Series. *Cryst. Growth Des.* **2013**, *13*, 3651−3656.
(32) Laugier, J.; Bouchu, B. *CelRef*; Laboratoire des Materiaux et du Génie Physique de l'Ecole Supérieure de Physique de Grenoble, 2003.
(33) Coelho, A. A. TOPAS and TOPAS-Academic: an Optimization Program Integrating Computer Algebra and Crystallographic Objects Written in C++. *J. Appl. Crystallogr.* **2018**, *51*, 210−218.
(34) *Bruker APEX3 v2019.1−0 - Crystallography Software Suite Bruker*; Bruker Axs, Inc., 2019.
(35) *SADABS - Area Detector Absorption Correction*; Bruker Axs, Inc., 2010.
(36) *SAINT V8.40A*; Bruker Axs, Inc., 2019.
(37) Sheldrick, G. M. SHELXT - Integrated Space-Group and Crystal-Structure Determination. *Acta Crystallogr. A* **2015**, *71*, 3−8.
(38) Sheldrick, G. M. Crystal Structure Refinement with SHELXL. *Acta Crystallogr.* **2015**, *C71*, 3−8.
(39) Farrugia, L. J. WinGX and ORTEP for Windows: An Update. *J. Appl. Crystallogr.* **2012**, *45*, 849−854.
(40) Macrae, C. F.; Sovago, I.; Cottrell, S. J.; Galek, P. T. A.; McCabe, P.; Pidcock, E.; Platings, M.; Shields, G. P.; Stevens, J. S.; Towler, M.; et al. Mercury 4.0: from visualization to analysis, design and prediction. *J. Appl. Crystallogr.* **2020**, *53*, 226−235.
(41) Bielecki, A.; Burum, D. P. Temperature Dependence of 207 Pb MAS Spectra of Solid Lead Nitrate. An Accurate, Sensitive Thermometer for Variable-Temperature MAS. *J. Magn. Res. A* **1995**, *116*, 215−220.
(42) Blahut, J. Solid-State NMR Dataset for Publication about Nicotinamide-Adipic Ac. Cocrystals. *Zenodo* **2025**, DOI: 10.5281/zenodo.15704838.
(43) Pickard, C. J.; Mauri, F. All-Electron Magnetic Response with Pseudopotentials: NMR Chemical Shifts. *Phys. Rev. B* **2001**, *63*, 245101−2451026.
(44) Yates, J. R.; Pickard, C. J.; Mauri, F. Calculation of NMR Chemical Shifts for Extended Systems Using Ultrasoft Pseudopotentials. *Phys. Rev. B* **2007**, *76*, 024401.
(45) Clark, S. J.; Segall, M. D.; Pickard, C. J.; Hasnip, P. J.; Probert, M. I. J.; Refson, K.; Payne, M. C. First Principles Methods Using CASTEP. *Z. Kristallogr.* **2005**, *220*, 567−570.
(46) Perdew, J. P.; Burke, K.; Ernzerhof, M. Generalized Gradient Approximation Made Simple. *Phys. Rev. Lett.* **1996**, *77*, 3865−3868.
(47) Vanderbilt, D. Soft Self-Consistent Pseudopotentials in a Generalized Eigenvalue Formalism. *Phys. Rev. B* **1990**, *41*, 7892−7895.
(48) Monkhorst, H. J.; Pack, J. D. Special Points for Brillouin-Zone Integrations. *Phys. Rev. B* **1976**, *13*, 5188−5192.
(49) Tkatchenko, A.; Scheffler, M. Accurate Molecular Van Der Waals Interactions from Ground-State Electron Density and Free-Atom Reference Data. *Phys. Rev. Lett.* **2009**, *102*, 073005−073009.
(50) Bernardes, C. E. S.; Feliciano, I. O.; Naese, C.; Emmerling, F.; Minas da Piedade, M. E. Energetics of Dehydroepiandrosterone Polymorphs I and II From Solution and Drop-Sublimation Calvet Microcalorimetry Measurements. *J. Chem. Thermodyn.* **2023**, *186*, 107137−107144.
(51) Bernardes, C. E. S. CBCAL: A Data Collection Program for Calorimetry Experiments (Version 3.0). *Zenodo* **2022**, DOI: 10.5281/zenodo.6475251.
(52) Bernardes, C. E. S. EASY GRAPH II - Making Data Plotting and Analysis Easier (2.1.24.1). *Zenodo* **2024**, DOI: 10.5281/zenodo.7061809.
(53) Wagman, D. D.; Evans, W. H.; Parker, V. B.; Schumm, R. H.; Halow, I.; Bailey, S. M.; Churney, K. L.; Nuttall, R. L. The NBS Tables of Chemical Thermodynamics Properties. *J. Phys. Chem. Ref. Data* **1982**, *11*, Supplement no. 12.
(54) Prohaska, T.; Irrgeher, J.; Benefield, J.; Böhlke, J. K.; Chesson, L. A.; Coplen, T. B.; Ding, T.; Dunn, P. J. H.; Gröning, M.; Holden, N. E.; et al. Standard Atomic Weights of the Elements 2021 (IUPAC Technical Report). *Pure Appl. Chem.* **2022**, *94*, 573−600.
(55) Perlovich, G. Melting Points of One- and Two-component Molecular Crystals as Effective Characteristics for Rational Design of Pharmaceutical Sgystems. *Acta Crystallogr. B* **2020**, *76*, 696−706.
(56) Schultheiss, N.; Newman, A. Pharmaceutical Cocrystals and Their Physicochemical Properties. *Cryst. Growth Des.* **2009**, *9*, 2950−2967.
(57) Feliciano, I. O.; Bernardes, C. E. S.; Minas da Piedade, M. E. Standard Molar Enthalpy of Sublimation of Form I Nicotinamide. *J. Chem. Thermodyn.* **2023**, *182*, 107042−107047.
(58) Joseph, A.; Bernardes, C. E. S.; Druzhinina, A. I.; Varushchenko, R. M.; Nguyen, T. Y.; Emmerling, F.; Yuan, L.; Dupray, V.; Coquerel, G.; da Piedade, M. E. M. Polymorphic Phase Transition in 4′-Hydroxyacetophenone: Equilibrium Temperature, Kinetic Barrier, and the Relative Stability of $Z' = 1$ and $Z' = 2$ Forms. *Cryst. Growth Des.* **2017**, *17*, 1918−1932.
(59) Threlfall, T. L. Turning DSC Charts of Polymorphs into Phase Diagrams: A Tutorial Paper. *Org. Process Res. Dev.* **2009**, *13*, 1224−1230.
(60) Simoes, R. G.; Bernardes, C. E. S.; da Piedade, M. E. M. Polymorphism in 4-Hydroxybenzaldehyde: A Crystal Packing and Thermodynamic Study. *Cryst. Growth Des.* **2013**, *13*, 2803−2814.
(61) Bond, A. D. A Survey of Thermal Expansion Coefficients for Organic Molecular Crystals in the Cambridge Structural Database. *Acta Crystallogr. B* **2021**, *77*, 357−364.

Downloaded from http://pubs.acs.org/cgdefu/article-pdf/26/14/5618/6521451/acs.cgd.6c00576.pdf by UNIV DEGLI STUDI DI PARMA user on 27 July 2026

https://doi.org/10.1021/acs.cgd.6c00576
Cryst. Growth Des. 2026, 26, 5618−5628